Optimal Design of Rotor Blades for an Axial Compressor Using the Gradient Based Method

Hyung-Jin Kim[1], Hyeon-Jae Noh[1], and Youn-Jea Kim[2(✉)]

[1] Graduate School of Mechanical Engineering, Sungkyunkwan University, Suwon, Republic of Korea
[2] School of Mechanical Engineering, Sungkyunkwan University, Suwon, Republic of Korea
yjkim@skku.edu

Abstract. Design optimization methods for rotor blades of an axial compressor have been developed by using the computational fluid dynamics (CFD). In order to improve the aerodynamic performances, such as pressure ratio and adiabatic efficiency, three-dimensional Reynolds averaged Navier-Stokes analysis was used for the single stage axial compressor. The optimum design process considering the aerodynamic characteristics consists of designing the shape using the Non-Uniform Rational B-Spline (NURBS) function and performing the optimum design with Gradient-Based Optimization Method (GBOM). For the proceeding of automated optimization, the commercial code ANSYS CFX ver. 16.1 and Design Exploration were applied. Results show that the newly designed model demonstrated better performance than the reference model. In particular, the pressure ratio was found to be higher than that of the reference model.

Keywords: Optimization · Axial compressor · CFD · Stacking line GBOM

1 Introduction

Turbomachinery is actively used throughout an industry in mechanical engineering. Especially, axial compressors, which can be seen as typical turbomachines, are actively used in aircraft engines and hybrid power generation facilities due to their characteristics. Replicating the flow in the gas turbine has many difficulties due to the complex flow in the gas turbine. In the case of gas turbine, high temperature and high pressure air pass through the compressor and combustor rotates the turbine through the stator and rotor of the turbine. Therefore, it is difficult to predict numerically, over a wide velocity range from subsonic to supersonic. Because of this difficulty, manufacturers of the compressor in the past have made initial design using the own data at the time of designing the compressor, and a final shape has been determined using experimental methods such as a wind tunnel [1]. As CFD began to develop in earnest in the 1970s, CFD techniques were used in designing the compressor from the middle-1970s. Algorithms have also been developed to derive features that will satisfy a particular purpose in conjunction with optimal design techniques based on a theory of optimization. Through the optimum design method, the designer can design the turbo machine

H. C. Rodrigues et al. (Eds.): *EngOpt 2018 Proceedings of the 6th International Conference on Engineering Optimization*, pp. 498–509, 2019.
https://doi.org/10.1007/978-3-319-97773-7_45

shape with the desired performance with less cost and time, and it is possible to derive the optimum shape more quickly due to the rapid development of the computer technology. However, since the optimization method requires several iterations to be performed, it is necessary to satisfy a plurality of constraints or a large computation time if the nonlinearity of the objective function is large. Despite these drawbacks, design fields based on the optimization theory have been developed by many researchers. Hicks and Henne have performed the optimal design of an airfoil based on the GBOM [2]. The Gradient Based Method has been widely used, which is a method of finding the direction using the first derivative of the objective function. Kammerer uses this method to optimize the design of the blade geometry of the multi stage turbine [3]. Catalano and Dadone have optimized the 2-D transonic cascade using the GBOM [4].

In this study, the shape of transonic blades was optimized by the GBOM. In addition, the effect of optimized blade configuration on flow behavior was investigated and its effect on performance improvement was investigated.

2 Numerical Study

2.1 Governing Equations

As equations of motion for transient fluid flow, Unsteady Reynolds Averaged Navier-Stokes (URANS) Equations reduce the computational effort compared to a direct numerical simulation (DNS). Their equations are generally adopted for practical engineering calculations [5]. The URANS equations are used to describe unsteady turbulent flows.

For unsteady compressible turbulent flows, the continuity, momentum, and energy equations are represented as follows:

$$\frac{\partial \rho}{\partial t} + \frac{\partial}{\partial x_j}\left(\rho \widetilde{u_j}\right) = 0 \tag{1}$$

$$\frac{\partial \rho \widetilde{u_l}}{\partial t} + \frac{\partial}{\partial x_j}\left(\rho \widetilde{u_l}\widetilde{u_J}\right) = -\frac{\partial \tilde{p}}{\partial x_i} + \frac{\partial \tau_{ji}}{\partial x_j} \tag{2}$$

$$\frac{\partial \rho H}{\partial t} - \frac{\partial p}{\partial t} + \frac{\partial}{\partial x_j}\left(\rho \widetilde{u_J} H\right) = \frac{\partial}{\partial x_j}\left(\Gamma \frac{\partial \tilde{T}}{\partial x_j}\right) + \frac{\partial}{\partial x_j}\left(\widetilde{u_l}\tau_{ji}\right) \tag{3}$$

where ρ, τ, H and Γ are density, the stress tensor, total enthalpy and thermal diffusivity. $\widetilde{u_l}$ are instantaneous velocity vector components and $\tilde{p}$ is instantaneous pressure.

2.2 Turbulence Model

A shear stress transport (SST) turbulence model based a k-ω model was used to numerically analyze an internal flow field of the axial compressor. The SST model combines advantages of the k-ω model and a k-ε model. The k-ω model is used near a

wall and the k-ε model is used in other areas. The SST model is known to be quite effective in predicting flow separation due to adverse pressure gradient [6]. In addition, the SST model used in this study has been reported to be superior to simulating turbulence fields near walls resulting from the flow separation. The SST model modifies turbulent viscosity by enhancing turbulent shear stress due to continuous turbulent energy perturbations in boundary layers. This modification improves the adverse pressure gradient and ability to simulate flow separation prediction.

2.3 Reference Model

The axial compressor model using NASA stage 37 operates at a speed of 17,188.7 rpm. Total pressure ratio and adiabatic efficiency are 1.771 and 86.374%, respectively, at the design mass flow rate of 20.19 kg/s. The tip clearance is 0.356 mm, the choking mass flow is 20.93 kg/s, and the near-stall point is 0.925 of the choke flow. Detailed parameters of the stage 37 are summarized in Table 1. An overall configuration is illustrated in Fig. 1. To optimize the shape of the axial compressor, performance was evaluated using the adiabatic efficiency, pressure ratio, which is commonly used in the dealing compressor. If the temperature increase is not significant, the specific heat for a certain pressure is almost constant at the inlet and the outlet, so the adiabatic efficiency is used as an objective function.

$$\eta_{ad} = \frac{\left(\frac{p_{0\ outlet}}{p_{0\ inlet}}\right)^{\frac{\gamma-1}{\gamma}} - 1}{\left(\frac{T_{0\ outlet}}{T_{0\ inlet}}\right) - 1} \tag{4}$$

$$p_r = \frac{p_{0\ outlet}}{p_{0\ inlet}} \tag{5}$$

Table 1. Design parameters of stage 37.

Parameters	Value
Number of rotor blades	36
Corrected rotation speed [rpm]	17188.7
Corrected mass flow rate [kg/s]	20.19
Tip speed [m/s]	454.14
Tip clearance size [mm]	0.36
Tip solidity	1.29
Hub relative inlet Mach number	1.13
Blade aspect ratio	1.19
Inlet hub-tip ratio	0.70

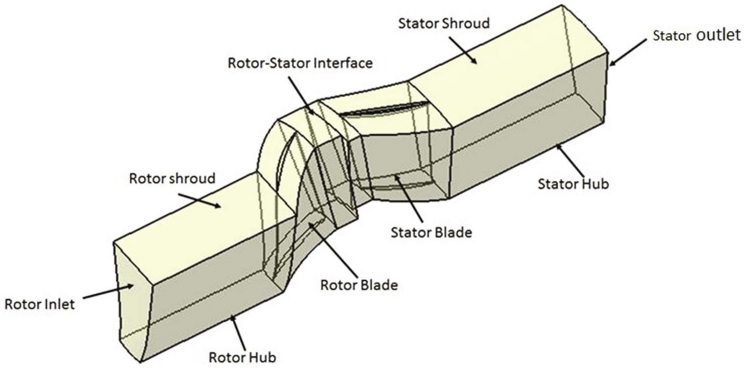

Fig. 1. Reference model of NASA stage 37.

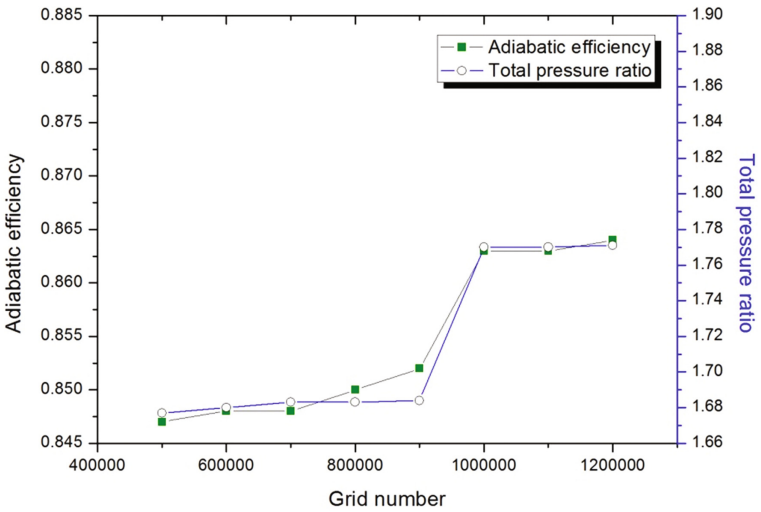

Fig. 2. Results of the grid dependency tests.

where η_{ad} refers to the adiabatic efficiency indicating the degree of adiabatic compression, and p_0 and T_0 denote the total pressure and total temperature, respectively (Fig. 2).

2.4 Boundary Conditions

The axial compressor model using NASA stage 37 operates at a speed of 17,188.7 rpm. Total In the case of analysis for a single blade used in the axial compressor, flow boundary conditions of an inlet and an outlet, periodic boundary conditions in pitch directions, and wall boundary conditions are applied. Generally, the inlet determines an angle of attack, pressure, and velocity of the flow field, and determines the pressure and

Table 2. Boundary conditions applied in this study.

Inlet total temperature	288.15 K
Inlet total pressure	1 atm
Outlet mass flow rate	20.19 kg/s
Interface	Frozen rotor, periodic

temperature at the outlet [7]. Total pressure and total temperature were specified at the inlet boundary conditions, and the mass flow rate was set to the outlet boundary conditions, as shown in Table 2.

2.5 Grid Dependency Test

Figure 1 shows effects of computational grids on the performance curves for the adiabatic efficiency and total pressure ratio. As shown in the Fig. 1, values of the adiabatic efficiency and total pressure ratio almost do not change over grid numbers of 900,000. Consequently, the optimum number of girds in the flow field was found to be 1 million.

3 Optimization Method

3.1 Geometry Definition

The NURBS used to create blade configurations include the following B-spline blending functions:

$$N_{i,0}(s) = \begin{pmatrix} 1 & if\ s_i \le s < s_{i+1} \\ 0 & otherwise \end{pmatrix} \tag{6}$$

$$N_{i,k}(s) = \frac{(s - s_i)N_{i,k-1}(s)}{s_{i+k-1} - s_i} + \frac{(s_{i+k} - s)N_{i+1,k-1}(s)}{s_{i+k} - s_{i+1}} \tag{7}$$

where, $N_{i,k}(s)$ denotes the blending function for a B-spline, and k is the local degree of the polynomial functions. The s_i is a knot value, which is a parameter value that represents the boundary value of a range in which each blending function has a value other than 0, when the range of the parameter 's' is divided into several sections. In the case of NURBS, the spacing may be non-uniform [8]. Figure 3 shows the blades generated by the NURBS.

3.2 Design Parameters

For design optimization, it is important to find the feasible and practical design space [9]. In this study, the geometric parameters of the rotor blade were selected as optimization design variables. Three design variables were derived from the layers of the layers of the blade as shown in Fig. 4: the number of rotor blades (N), 50% span angle (θ_1), and shroud angle (θ_2). The design variables were set with reference to the

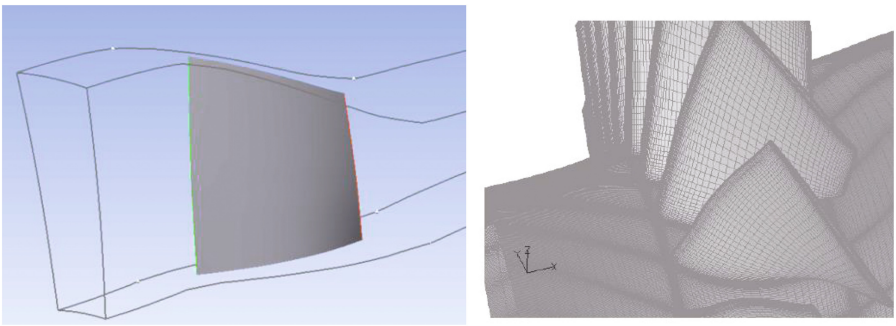

Fig. 3. Blade geometry with NURBS surfaces.

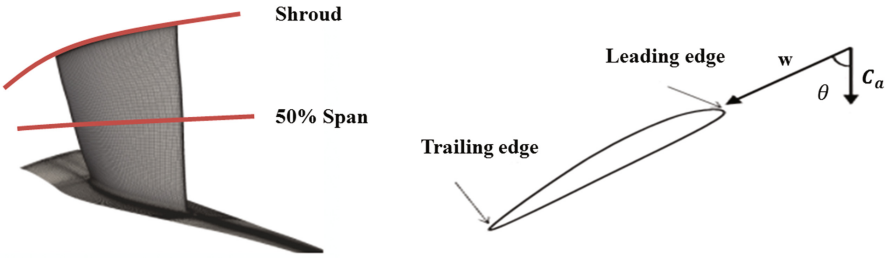

Fig. 4. Design variables in NASA stage 37.

previous study that adjusts blade stacking lines to improve the performance of the axial flow compressor [10].

3.3 Refinement of Design of Experiments

The refinement of design of experiments (DOE) is a necessary step of the optimization process using the reference model. After reducing the design space, the new design points have been recalculated with different design methods. The design points can be determined by using the central composite design (CCD) method. Consequently, it is possible to maximize the amount of information generated with a minimum number of CFD results. The CCD method consists of the following formula:

$$y = 2^k + 2k + 1 \tag{6}$$

where, y is the number of design points, and k is the number of parameters. Table 3 shows the results of DOE refinement.

3.4 Gradient-Based Optimization Method

Several methods have been developed for the numerical optimization of nonlinear problems, but there is no significant difference in the optimal solutions [11]. In this

Table 3. Results for the design of experiment.

	θ_1 [°]	θ_2 [°]	N	η_{ad}	p_r
1	−6.79	−6.22	36	86.374	1.771
2	−6.79	−6.22	37	86.357	1.752
3	−6.79	−6.22	35	86.694	1.802
⋮	⋮	⋮	⋮	⋮	⋮
13	−6.79	−6.22	38	85.740	1.734
14	−7.43	−6.74	39	92.980	1.855
15	−6.96	−6.50	36	86.532	1.771

study, the GBOM is used which has the advantage of finding the optimal solution quickly with a small number of calculations [12]. The purpose of the GBOM is to search a minimum of a dimensional target function $f(\vec{x})$. The target function is approximated by a terminated Taylor series expansion around $\overrightarrow{x_0}$. Unconstrained gradient-based optimization can be described as follows [13, 14]:

1. The iterative calculation starts with iteration number k = 0 and a starting point, x_k.
2. The test for convergence should be carried out. If the conditions for convergence are satisfied, the iterative calculation is stopped, and the solution obtained at that time becomes the optimum solution.
3. A vector p_k that defines the direction of the n-space to be used in the design should be calculated.
4. Calculation of the step length is required, and a positive scalar, α_k, such that $f(x_k + \alpha_k p_k) < f(x_k)$, should be derived
5. The design variables must be updated and configured, as follows:

$$x_{k+1} = x_k + \alpha_k p_k, \quad k = k+1, \quad x_{k+1} = x_k + \underbrace{\alpha_k p_k}_{\Delta x_k} \tag{7}$$

The function $f(\mathrm{x})$, where x is the n-vector, $\mathrm{x} = [x_1, x_2, \cdots, x_n]^T$, should be reviewed. The gradient vector of this function is given by the partial derivatives with respect to each of the independent variables:

$$\nabla f(\mathrm{x}) \equiv g(x) \equiv \begin{bmatrix} \frac{\partial f}{\partial x_1} \\ \frac{\partial f}{\partial x_2} \\ \vdots \\ \frac{\partial f}{\partial x_n} \end{bmatrix} \tag{8}$$

In the multivariate case, the gradient vector is perpendicular to the hyperplane tangent to the contour surfaces of constant f. Higher derivatives of multi-variable functions are defined as in the single-variable case, but for each differentiation, the number of gradient components increases by a factor of n. While the gradient of a

function of n variable is an n-vector, the second derivative of an n-variable function is defined by n^2 partial derivatives.

$$\frac{\partial^2 f}{\partial x_i \partial x_j}, i \neq j \text{ and } \frac{\partial^2 f}{\partial x_i^2}, \ i = j \tag{9}$$

If the partial derivatives $\partial f/\partial x_i$, $\partial f/\partial x_j$, and $\partial^2 f/\partial x_i \partial x_j$ are continuous, and f is single-valued, $\partial^2 f/\partial x_i \partial x_j$ exists. Therefore, the second order partial derivatives can be represented by a square symmetric matrix, called the Hessian matrix:

$$\nabla^2 f(x) \equiv H(x) \equiv \begin{bmatrix} \frac{\partial^2 f}{\partial^2 x_1} & \cdots & \frac{\partial^2 f}{\partial x_1 \partial x_n} \\ \vdots & \ddots & \vdots \\ \frac{\partial^2 f}{\partial x_n \partial x_1} & \cdots & \frac{\partial^2 f}{\partial^2 x_n} \end{bmatrix} \tag{10}$$

This contains $n(n+1)/2$ independent elements. If f is constant, the function can be expressed as:

$$f(x) = \frac{1}{2} x^T H x + g^T x + \alpha \tag{11}$$

As in the single variable case, the optimality conditions can be derived from the Taylor-series expansion of f about x^*:

$$f(x^* + \varepsilon p) = f(x^*) + \varepsilon p^T g(x^*) + \frac{1}{2} \varepsilon^2 p^T H(x^* + \varepsilon \theta p) p \tag{12}$$

where, $0 \leq \theta \leq 1$, ε is a scalar, and p is an n-vector.

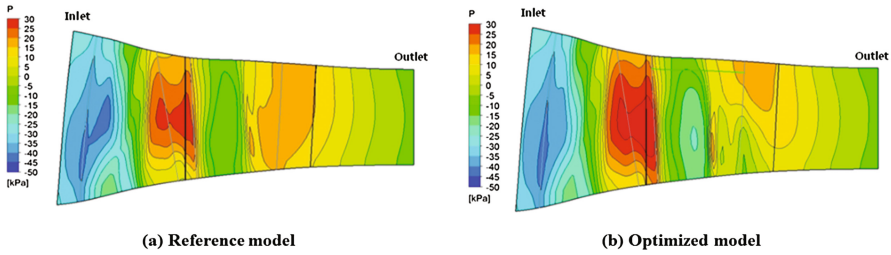

(a) Reference model **(b) Optimized model**

Fig. 5. Pressure contours at the meridional plane.

4 Results and Discussion

4.1 Results of Reference Model

The performance factors of the axial compressor were calculated. The adiabatic efficiency was 86.374% and the pressure ratio was 1.771. Figure 5 shows the pressure distribution at the meridian. It was confirmed that the pressure rises from the inlet to the outlet of the rotor.

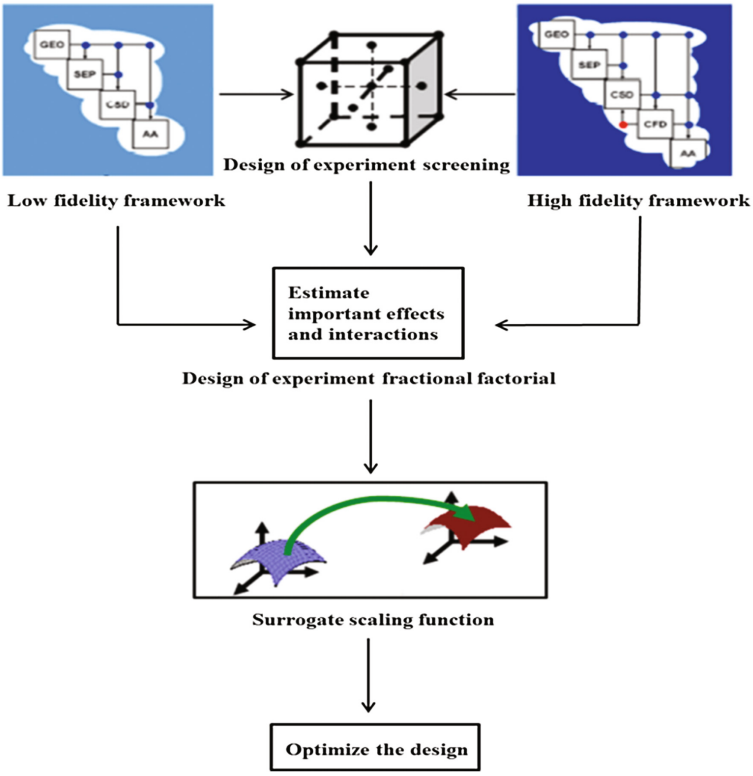

Fig. 6. Optimization flow chart in this study.

4.2 Results of Optimization

Figure 6 shows that the optimal model is derived by the gradient method which is one of the local optimization methods. Since this is an optimal point based on an approximate model, the relative error is evaluated by comparing it with the output variable value that is directly calculated by numerical analysis. Table 4 shows that the relative error between the approximate model of adiabatic efficiency by the GBOM and the CFD result occurred at 0.018%, and the pressure ratio showed a difference of 0.216%. All output variables showed high fitness with the approximate model, and the

Table 4. Comparison results between the GBOM and CFD.

	θ_1 [°]	θ_2 [°]	N	η_{ad}	p_r
GBOM	−7.43	−6.74	39	92.980	1.855
CFD				92.963	1.851

pressure ratio was most accurately predicted. As a result, it can be deduced that the fit of the approximate model of adiabatic efficiency is very high.

Table 5. Comparison results between the reference model and the optimal model.

	θ_1 [°]	θ_2 [°]	N	η_{ad}	p_r
Reference model	−6.79	−6.22	36	86.374	1.771
Optimal model	−7.43	−6.74	39	92.980	1.855

Table 5 compares the results of the reference model and the optimal model. As a result of the optimum design, the adiabatic efficiency, which is the main performance parameter of the objective function and the axial compressor, is increased by about 7.10%. The pressure ratio is increased by 4.53%. Analyzing the flow phenomenon at the trailing edge between the initial shape and the optimal shape of the subsonic axial compressor, the flow separation at the trailing edge of the optimum shape is weakened, and the entropy distribution shows that the entropy generation is reduced not only in the trailing edge, but also in the rotor blade as a whole, as shown in Fig. 7.

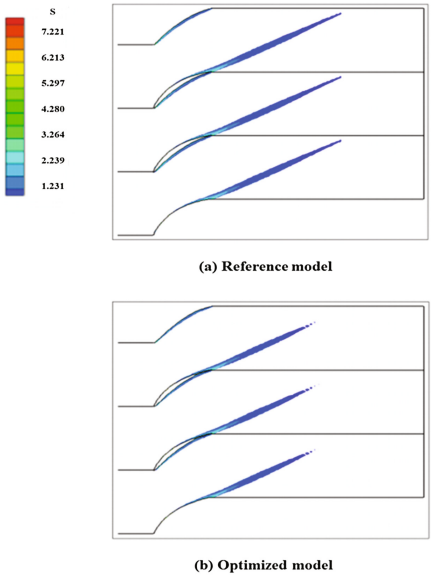

Fig. 7. Entropy distribution at 50% span.

The negative sweep forward configuration will have a long path near the shroud area that will accelerate the flow, which will reduce load on the shroud, which will be useful for the rotor blade. The blades area of the reference model will be more loaded, due to the lower skew, and fewer blades than the end wall sections. Therefore, the optimal model will lead to the appropriate span section area, producing better improvement.

5 Conclusions

In this study, the shape of an axial flow compressor rotor was optimized three-dimensionally. In the optimum design process, the design parameters of the axial compressor were selected by analyzing the correlation between the design variables and performance, by using the refinement of DOE, NURBS function, and the GBOM. As a result of the shape optimization, the optimum model showed a 4.53% increase in the pressure ratio, and a 7.10% increase in the adiabatic efficiency over the basic model.

References

1. Marshall, J.G., Imregun, M.: A review of aeroelasticity methods with emphasis on turbomacinery applications. J. Fluids Struct. **10**(3), 237–267 (1996)
2. Hicks, R.M., Henne, P.A.: Wing design by numerical optimization. J. Aircr. **15**(7), 407–412 (1978)
3. Kammerer, S., Mayer, J.F., Paffrath, M., Wever, U., Jung, A.R.: Three-dimensional optimization of turbomachinery bladings using sensitivity analysis. In: ASME Turbo Expo, GT2003-38037 (2003)
4. Catalano, L.A., Dadone, A.: Orthogonal shape functions and progressive optimization for the design of 2-D transonic cascades. In: Proceedings of ASME Turbo Expo 2002, GT-2002-30678 (2002)
5. Reynolds, O.: On the dynamical theory of incompressible viscous fluids and the determination of the criterion. Philos. Trans. R. Soc. Lond. A **186**, 123–164 (1895)
6. Menter, F.R.: Two-equation eddy-viscosity turbulence models for engineering application. AIAA J. **32**(8), 1598–1605 (1994)
7. Dalbert, P., Wiss, D.H.: Numerical transonic flow field predictions for NASA compressor rotor 37. In: The American Society of Mechanical Engineers, vol. 45, pp. 1–12 (1995)
8. Wahid, S.G., Temesgen, T.M.: Optimal geometric representation of turbomachinery cascades using NURBS. Inverse Probl. Sci. Eng. **11**(5), 359–373 (2003)
9. Cai, N., Xu, J.H.: Aerodynamic-aeroacoustic performance of parametric effects for skewed-swept rotor. ASME paper 2001-GT-0354 (2001)
10. Jang, C.M., Samad, A., Kim, K.Y.: Optimal design for stacking line of rotor blade in a single-stage transonic axial compressor. KSFM J. Fluid Mach. **9**(3), 7–13 (2006). (in Korean)
11. Haug, E.J., Arora, J.S.: Applied Optimal Design Mechanical and Structural Systems, pp. 77–89. Wiley Interscience, New York (1979)

12. Sohoni, V.N., Arora, J.S., Haug, E.J.: A general Purpose Nonlinear Programming Computer Code GRP Based on the Gradinet Projection Method. TN-41, University of Iowa (1978)
13. Belegundu, A.D., Chandrupatla, T.R.: Optimization Concepts and Applications in Engineering. Prentice Hall, Upper Saddle River (1999)
14. Nocedal, J., Wright, S.J.: Numerical Optimization. Springer, New York (2006)